sustainability

MDPI

Article

Evaluating the Fast Frequency Support Ability of the Generation Units in Modern Power Systems

Muyang Liu [1], Ruo Mo [1], Yening Lai [2], Zhaowei Li [1], Zhaohui Qie [2] and Hua Zheng [1,*]

[1] Department of Electrical Engineering, North China Electric Power University, Beijing 102206, China; muyang.liu@xju.edu.cn (M.L.); moruo96@stu.xju.edu.cn (R.M.)
[2] State Grid Electric Power Research Institute, Nanjing 250003, China
* Correspondence: zhenghua@ncepu.edu.cn

Abstract: Modern power systems include synchronous generators (SGs) and inverter-based resources (IBRs) that provide fast frequency support (FFS) to the system. To evaluate the FFS ability of both SGs and IBRs under a unified framework, this paper proposes a method that evaluates the FFS ability of each generation unit via its dynamic trajectories of the active power output and the frequency following a contingency. The proposed method quantified FFS ability via two indexes, namely, the equivalent inertia constant and the equivalent droop, of each generation unit. The Tikhonov regularization algorithm is employed to estimate the FFS ability indexes. The New England 10-machine system serves to validate the feasibility and accuracy of the proposed method and illustrate the different FFS ability of the grid−forming and grid−following IBRs.

Keywords: fast frequency support; equivalent inertia constant; virtual droop constant; grid−foaming control

Citation: Liu, M.; Mo, R.; Lai, Y.; Li, Z.; Qie, Z.; Zheng, H. Evaluating the Fast Frequency Support Ability of the Generation Units in Modern Power Systems. *Sustainability* **2024**, *16*, 2506. https://doi.org/10.3390/su16062506

Academic Editor: Mohamed A. Mohamed

Received: 4 January 2024
Revised: 14 February 2024
Accepted: 1 March 2024
Published: 18 March 2024

1. Introduction

With the increasingly high penetrations of inverter-based resources (IBRs), the rotation inertia level and frequency regulation reserve become inadequate in modern power systems. To face this challenge, with the developing power electronics control techniques such as virtual synchronous generator (VSG) [1–4], virtual inertia, and virtual droop [5,6], some IBRs can now provide fast frequency support (FFS) to the power system. FFS means the active power that is injected into the power system following the frequency event, which is mainly boosted by the rotational inertia and primary frequency control (PFC) of synchronous generators (SGs) in traditional power systems. In modern power systems, the dynamic active power regulation of the IBR within the timescale of the PFC is regarded as the FFS from the IBR. This paper targets developing a unified evaluation method for the FFS ability of both SGs and IBRs. In order to improve the utilization rate of renewable energy, the optimal techniques for building energy systems with renewable energy [7] and the risk control of mission-critical systems [8] are developed. The research content of this article provides a theoretical basis for the operation and control of the wind–photovoltaic–storage hybrid power system, therefore assisting renewable energies in gradually replacing fossil fuels in the power supply, benefiting worldwide sustainable development.

The FFS ability evaluation of the generation unit can be divided into two categories, namely, the precontingency and postcontingency evaluation. The precontingency method evaluates the FFS ability of the generation units according to their physical characteristics and the control parameters and is crucial for the schedule and operation of the power system. Reference [9] introduces a unified metric based on the physical characteristics that quantify the initial and sustaining energy that can be used to provide FFS to the grid. Reference [10] shows that inertial and droop metrics can demonstrate FFS ability after analyzing the features of the generation unit. Reference [11] proposes a quantitative index of frequency support capability based on the frequency safety binary table through the study of analytical modeling of wind turbines. In general, the precontingency FFS ability

for SGs can be represented as its rotational inertia and droop [12], while the evaluation method for IBRs is still a challenge.

The postcontingency evaluation method is based on the exact FFS from the generation unit during the occurred frequency evolution following a contingency. The postcontingency method is mainly used for clearing and paying for the frequency and/or inertia ancillary service [13,14]. A typical postcontingency evaluation method is the event-triggered online estimation of the inertia [15]. References [16,17] use the system inertia as a frequency support evaluation metric to reflect the dynamic process after system power perturbation.

However, the inertia, including both the rotational and virtual inertia, is not the only FFS that IBRs can provide [18]. Considering that the inverter control is much faster than the controllers of SGs, all the frequency control of the IBR that can regulate the active power output before the secondary frequency regulation of the SGs can be regarded as fast frequency control [19]. Reference [20] analyzes the characteristics of different IBRs under large disturbance accidents and proposes a metric system that considers both inertia and droop.

The FFS of the SG can be easily predicted according to precontingency evaluation. The FFS ability of IBRs, as discussed before, is hard to predict as it is affected by the ever-changing status of the renewable power generation and/or the state of charge of the energy storage system [21]. The evaluation of the FFS ability of the IBR is still highly reliant on the postcontingency analysis. However, a systematic method to track the FFS ability of the IBR online is still missing.

Based on the definitions and effects of the FFS from SGs, this paper proposes unified FFS ability indexes for both SGs and IBRs. The specific contributions of this paper are as follows:

- A comprehensive review of the existing techniques of the FFS of the IBRs;
- Proposing the FFS ability indexes and the corresponding postcontingency evaluation method;
- A discussion of the different FFS abilities for different kinds of IBRs.

The remainder of the paper is organized as follows: Section 2 reviews the existing FFS control techniques of various IBRs. Section 3 proposes the FFS ability indexes and the corresponding evaluation methods for the indexes. The well-known New England 10-machine system serves to validate the accuracy of the proposed FFS evaluation method in Section 4. Section 4 also discusses the different FFS abilities of different IBRs based on the proposed evaluation method. Conclusions are drawn in Section 5.

2. Technical Background: Fast Frequency Support for Modern Power System

2.1. The Timescale of FFS

Figure 1 shows a typical frequency evolution of a modern power system following a frequency event. As we can see in Figure 1, according to the different dominant frequency responses of the system, the evolution can be divided into three phases, namely, the inertia response period (T_{inertia}), the PFC period (T_{PFC}), and the secondary frequency control (SFC) period (T_{SFC}). These three phases are decided by the frequency responses of the synchronous generators, which are the main frequency regulation sources in the traditional power system. In a modern power system with inverter-based resources (IBRs) participating in the frequency regulation, the FFS refers to the frequency response within the timescale of T_{inertia} and T_{PFC} [22].

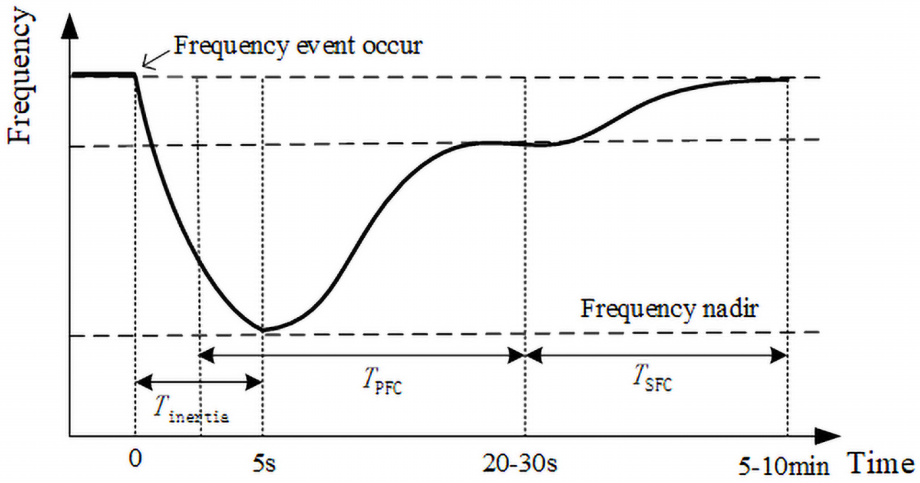

Figure 1. A typical frequency evolution.

With the power electronic control techniques, the IBR can respond to the frequency deviation of the grid within milliseconds and boost active power according to the specific control strategies. The following subsection provides a detailed review of the FFS from IBRs.

2.2. FFS Control Techniques of IBRs

According to the different grid connection techniques, the IBR can be divided into two categories, namely, the grid−following IBR and the grid−forming IBR [23].

2.2.1. Grid−Following IBR with FFS

The IBR with grid−following control, abbreviated as GFL, detects the frequency deviation of the power system via the phase-locked loop (PLL). Figure 2 shows the typical structure of the GFL with FFS. In Figure 2, ω^* is the frequency reference; ω_{PLL} is the output frequency of the PLL; V^* and V_d are the references of the control voltage of the GFL and the d-axis components of the voltage at the point of common coupling (PCC), respectively; K_d and K_M are the proportional and differential coefficients in the virtual inertia control, respectively; K_q is the droop gain of the voltage droop control; and p^* and q^* are the references of the active power and reactive power control, respectively.

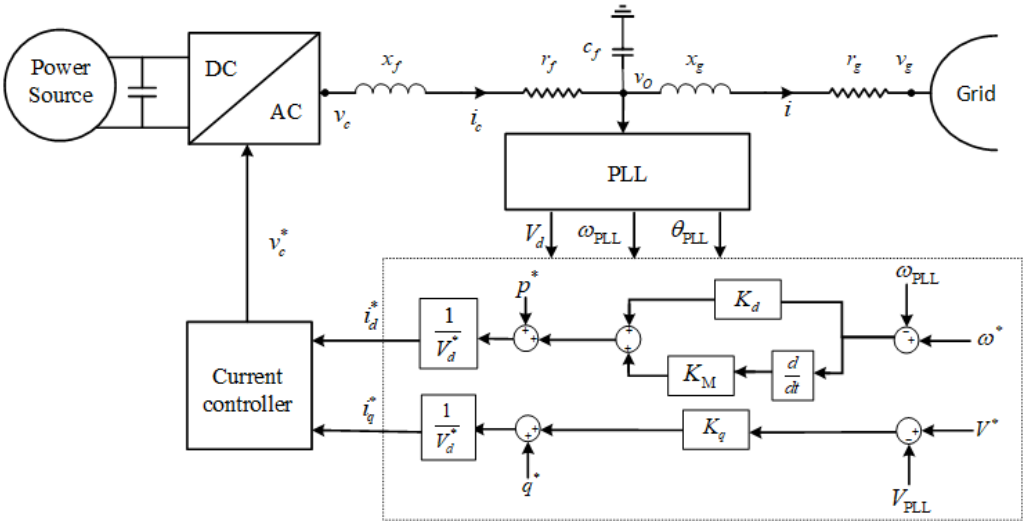

Figure 2. Grid−following control.

As we can see in Figure 2, the GFL provides FFS according to the frequency deviation and rate of change of frequency (RoCoF) measured by the PLL. The virtual inertia control

with the control gain K_M regulates the active power output by adjusting the reference of the inner current loop. In this context, the equivalent inertia constant of the GFL with virtual inertia highly depends on the selection of K_M. The active power control with the control gain K_d responds to the frequency deviation that simulates the droop control of the SG. The control effect, therefore, can be evaluated by a virtual droop gain that will be around K_d while being affected by the dynamics of the GFL that differs from the SG. The details of the GFL dynamics are discussed in [24].

The power source at the DC side in Figure 2 can be energy storage or renewable sources. The category of the power source and its power output features can decide the capability of the FFS of this IBR by limiting the selection range of K_M and K_d.

2.2.2. Grid−Forming IBR with FFS

Similar to the GFL, the IBR with grid−forming control, abbreviated as GFM, can be implemented on the IBRs including energy storage systems and renewable sources.

The main difference between GFM and GFL is the synchronization technique. The GFM, similar to the SG, can control the output voltage and thus work as a voltage source in the grid. The GFM can regulate the active output power according to the phase angle deviations between its equivalent internal electric potential and the grid voltage, which allows for providing fast frequency support to the grid. The VSG is one of the most common control strategies of the GFM, which simulates the swing equation of the SG and provides virtual inertia to the grid. Figure 3 shows a typical GFM control scheme, where the VSG control acts as the outer loop of the inverter [25].

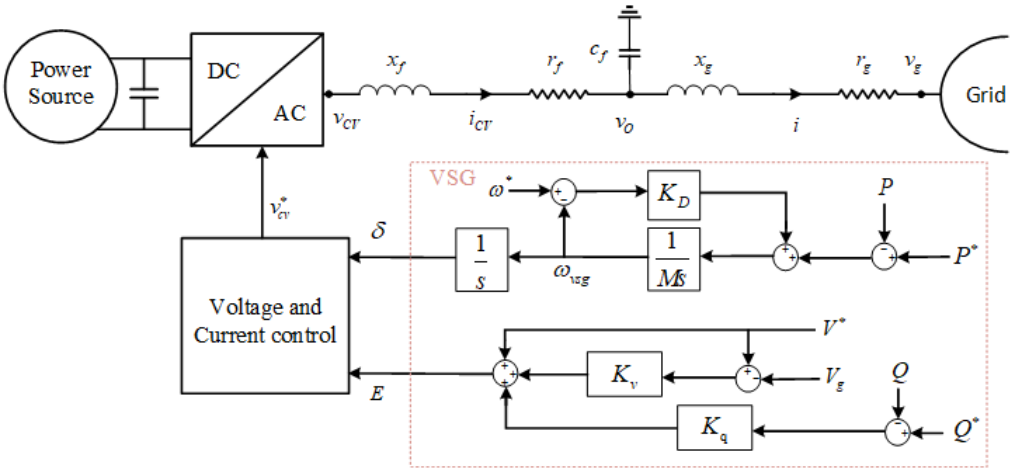

Figure 3. Grid−forming control.

According to Figure 3, the active regulation portion of the GFM provides virtual inertia and virtual droop gains to the system by the following equation:

$$M\frac{d\triangle\omega_{\text{vsg}}}{dt} = P^* - P_e + K_D(\omega^* - \omega_{\text{vsg}}), \tag{1}$$

where M is virtual inertia, P^* is the reference of the active power, P is the real power, K_D is virtual droop gains, ω^* is the frequency reference, and ω_{vsg} is the VSG frequency. Equation (1) is deduced from the classic swing equation [26]. Note that in some VSG implementations [27,28], damping and droop are not the same. In this case, the PLL needs to be added, which is more cumbersome. Thus, the FFS capability of the IBR can be determined by limiting the range of choices for M and K_D.

In Figure 3, δ is the phase difference between the GFM internal voltage and the grid voltage at the PCC. According to the current definition, we can say that in per-unit form, $\dot{\delta} = \omega_{\text{vsg}}$ and $\ddot{\delta}$ is the RoCoF. In voltage-reactive power control in GFM control, K_v is the voltage droop gain, K_q is the reactive power-voltage droop gain, V^* is the voltage reference,

V_g is the grid point voltage, Q^* is the reference of the reactive power, and Q is the real reactive power.

It is worth pointing out that the GFM frequency tuning response is much faster, so the frequency tuning ability will be better than the GFL.

3. Evaluation Method for the FFS Ability

3.1. Indexes of FFS Support Ability

According to the discussion in Section 2, the effects of FFS is to suppress the RoCoF, the maximal frequency deviation, and the error of the quasi-steady state following the PFC during the frequency evolution, as shown in Figure 1. For a traditional power system with the SG as the only source, these effects are from the rotational inertia and the PFC of the SG. In other words, the ability of the SG to suppress the RoCoF, maximal frequency deviation, and quasi-steady-state error can be evaluated by the equivalent inertia constant and the droop gain of the SG. In this context, the most straightforward indexes for the transmission system operator (TSO) to understand the FFS ability of an IBR can be the equivalent inertia constant of its virtual inertia and the equivalent droop gain of its active power control loop.

The definition of the equivalent inertia constant of the SG is derived from the swing equation of the synchronous generator, and its unit value is as follows:

$$2H_{SG}\dot{\omega}_{SG} = P_m - P_{e,SG}\,, \tag{2}$$

where H_{SG} is the inertia constant of the synchronous generator, $\dot{\omega}_{SG}$ is the rate of change of the angular frequency of the synchronous generator, P_m is the mechanical power of the synchronous generator, and $P_{e,SG}$ is the electromagnetic power injected into the grid. Following a frequency event, P_m can be regulated by the primary and secondary frequency controllers, namely, the turbine governor (TG) and the automatic generation regulator (AGC), and thus, we have the following:

$$P_m = P_{UC,SG} + P_{PFC,SG} + P_{SFC,SG}\,, \tag{3}$$

where $P_{UC,SG}$ is the power reference for the SG provided by the control and operation center through solving the economic dispatch for the power demand at this operation period, and $P_{PFC,SG}$ and $P_{SFC,SG}$ are the active power regulated by the TG and AGC, respectively.

Referring to Equation (2), we then deduce the definition of the equivalent inertia constant of an IBR providing virtual inertia to the system:

$$2H_{IBR}\dot{\omega}_{IBR} = \Delta P_{e,IBR}\,, \tag{4}$$

where H_{IBR} is the equivalent inertia constant of the IBR, and $\Delta P_{e,IBR}$ is the active power output boosted by the power electronic control following the frequency event. The definition of the ω_{IBR} of the GFM is the angular frequency of its internal voltage that was established, while the GFL performs as a current source with no internal voltage. Considering that the FFS control strategies of the GFL are fed by the frequency measured by the PLL, we can assume that the ω_{IBR} of the GFL is mathematically equal to the angular frequency obtained through the PLL.

Note that the IBR can also participate in the PFC and SFC of the power system. The PFC of the IBR represents the FFS control of the IBR that regulates the active power according to the local frequency deviation signal and can last through the whole PFC period of the power system. However, as a typical power electronics control, the PFC of the IBR can respond much faster than that of the SG. Referring to the fact the PFC effect of the SG can be quantified by the droop, we deduce the following definition of the equivalent virtual droop of the IBR:

$$P_{PFC,IBR} = K_{D,IBR}(\omega_{IBR} - \omega_N)\,, \tag{5}$$

where $K_{D,IBR}$ is the equivalent virtual droop of the IBR, ω_N is the nominal angular frequency, and $P_{PFC,IBR}$ is the active power boosted by the PFC of the IBR and a part of $\Delta P_{e,IBR}$ that cannot be measured directly.

It is important to note that as indexes for quantifying the FFS effect referring to the ability of SGs, the equivalent inertia constant and the equivalent active-power droop of an IBR may not numerically equal the virtual inertia constant and virtual droop gain in the control loop. The following subsections explain the method for computing the indexes of the FFS ability of an IBR via the measurable variables during the frequency evolution of the power system. Since the evaluating method of the indexes can be used for both the SG and the IBR, the subscripts of the variables are removed to present the generality.

3.2. Evaluating Equivalent Inertia Constant

To deduce the evaluating method of the equivalent inertia constant, we first differentiate the swing Equation (2):

$$2H\ddot{\omega} = \dot{P}_{UC} + \dot{P}_{PFC} + \dot{P}_{SFC} - \dot{P}_e \,. \tag{6}$$

Within the interval of power dispatch, there must be a constant P_{UC} for each source, which means $\dot{P_{UC}} = 0$. Considering the suitable time window to collect the dynamic data for the evaluation of the indexes of the *FFS* ability is the interval between the moment that the frequency event occurs and the moment that the system reaches the quasi-steady state following the PFC. Within this time window, it is reasonable to assume $\dot{P_{SFC}} = 0$. Particularly, during the $T_{inertia}$ shown in Figure 1, the dynamic behaviors of the generation unit were dominated by the equivalent inertia constant. We can therefore evaluate the equivalent inertia constant with the time window located in $T_{inertia}$, where we can assume that the variation of the active power output is mainly regulated by the inertial response of the source. In this context, we deduce that within $T_{inertia}$, there is the following:

$$2H \approx -\frac{\dot{P}_e}{\ddot{\omega}} \,, \tag{7}$$

where P_e is the active power output of the source that can be measured directly. References [29–31] prove that with the phasor measurement unit (PMU) installed at the point of interconnect (POI) of the power source, ω and $\dot{P}_e$ can be estimated accurately.

With the time series of ω and $\dot{P}_e$ estimated through the PMU, we can construct the following formula:

$$2H \approx 2H_j^* = \frac{\left|\dot{P}^*(t_j)\right|}{\left|\ddot{\omega}^*(t_j)\right|} \,, \tag{8}$$

where H_j^* is the estimated value of the virtual inertia constant at t_j time, $\dot{P}^*$ is the estimated value of active power at t_j time, and $\ddot{\omega}^*$ is the estimated value of the angular frequency at t_j time. Considering that the virtual inertia constant with the effect of inertia level must be positive, Equation (8) uses the absolute value to reduce the storage of sign bits during the evaluation.

To avoid the fractional structure that may introduce large errors in the evaluation according to [15], we rewrite (8) as follows:

$$\left|\ddot{\omega}^*(t_j)\right| \cdot 2H_j^* - \left|\dot{P}^*(t_j)\right| = \varepsilon_H \,, \tag{9}$$

where ε is the residual error resulting from the estimation error of H_j^*. The more accurate the H_j^*, the closer the ε to zero.

Consider a time window for the equivalent inertia estimation between the moment t_1 and t_J. We can have the chronological sequences formed by $\ddot{\omega}^*$ and $\dot{P}^*$ as follows:

$$A = 2[|\ddot{\omega}^*(t_1)|, |\ddot{\omega}^*(t_2)| \cdots |\ddot{\omega}^*(t_{J-1})|, |\ddot{\omega}^*(t_J)|]^T \tag{10}$$

$$b = [|\dot{P}^*(t_1)|, |\dot{P}^*(t_2)| \cdots |\dot{P}^*(t_{J-1})|, |\dot{P}^*(t_J)|]^T. \tag{11}$$

With Equations (9)–(11), we can set up a least square problem to find a relatively accurate H^* by minimizing the residual error for all measure data obtained within the time window:

$$H^* \text{ s.t. } \min(AH^* - b)^2 . \tag{12}$$

By introducing the Tikhonov regularization algorithm to solve the least square problem Equation (12) [32] and assuming $x = H^*$, we can construct the loss function of the Tikhonov regularization algorithm as follows:

$$L_{\mathrm{T}}(x) = \|Ax - b\|^2 + \lambda \|x\|^2 , \tag{13}$$

where λ is the regularization coefficient. The regularization coefficient λ controls the degree of regularization. If overfitting occurs, increasing the value of λ will increase the regularization penalty accordingly, and the overall loss function will not converge, thus skimming over data that can lead to overfitting.

We can obtain the most accurate H^* by minimizing $L_{\mathrm{T}}(x)$. With that goal, we compute the partial derivative of $L_{\mathrm{T}}(x)$ as follows:

$$\frac{\partial L_{\mathrm{T}}(x)}{\partial x} = 2\mathrm{A}^{\mathrm{T}}\mathrm{A}x - 2\mathrm{A}^{\mathrm{T}}\mathrm{b} + 2\lambda x . \tag{14}$$

At the minimal point, we must have $\frac{\partial L_{\mathrm{T}}(x)}{\partial x} = 0$. In this context, we can deduce the following:

$$x = \left(\mathrm{A}^{\mathrm{T}}\mathrm{A} + \lambda \mathrm{E}\right)^{-1} \mathrm{A}^{\mathrm{T}} b , \tag{15}$$

where E is the unit matrix. The above formula allows us to evaluate H^* through the measurable variables collected from the time window T_{inertia}.

3.3. Evaluating Virtual Droop Constant

With the evaluated equivalent inertia constant of the source, we can then propose the evaluating method for the virtual droop constant by combining Equations (4) and (5):

$$2H\dot{\omega} = K_D \Delta\omega - \Delta P_{\mathrm{e}} . \tag{16}$$

During the T_{PFC} shown in Figure 1, the dynamic behaviors of the generation unit were dominated by the virtual droop constant. We can therefore evaluate the virtual droop constant with the time window located in T_{PFC}, where we can assume that the variation of the active power output is mainly regulated by the PFC of the source. In this context, we deduce that within T_{PFC}, there is the following:

$$K_D = \frac{2H\dot{\omega} + \Delta P_{\mathrm{e}}}{\Delta\omega} . \tag{17}$$

Similar to the evaluating technique for the equivalent inertia constant, to avoid the fractional structure, at the specific moment t_n, we can rewrite Equation (17) as follows:

$$\Delta\omega^*(t_n) \cdot K^*_{D,n} - (2H^*\dot{\omega}^*(t_n) + \Delta P(t_n)^*) = \varepsilon_{\mathrm{D}} , \tag{18}$$

where H^* can be obtained through the method described in Section 4.2, and ε_{D} is the residual error resulting from the estimation error of K^*_D. To simplify the formula writing, assume that $\mathrm{Y}^*(t_n) = 2H^*\dot{\omega}^*(t_n) + \Delta P(t_n)^*$. Consider a time window for the equivalent

inertia estimation between the moment t_M and t_N. We can have the chronological sequences formed by $\Delta\omega^*$ and Y^* as follows:

$$C = [(\Delta\omega^*(t_M)), (\Delta\omega^*(t_{M+1})) \cdots (\Delta\omega^*(t_{N-1})), (\Delta\omega^*(t_N))]^T \tag{19}$$

$$d = [(\mathrm{Y}^*(t_M)), (\mathrm{Y}^*(t_{M+1})) \cdots (\mathrm{Y}^*(t_{N-1})), (\mathrm{Y}^*(t_N))]^T. \tag{20}$$

With the above equations, we can set up a least square problem to find a relatively accurate K_D^* by minimizing the residual error for all measure data obtained within the time window:

$$K^* \text{s.t.} \min(CK_D{}^* - d)^2, \tag{21}$$

where $K_D{}^*$ is the estimated value of the virtual droop constant, assuming $y = K_D{}^*$. By introducing the Tikhonov regularization algorithm to solve the least square problem Equation (21) and by referring to the evolution of the equivalent inertia constant, the formula for the virtual droop constant is finally obtained as follows:

$$y = \left(\mathrm{C}^{\mathrm{T}}\mathrm{C} + \lambda\mathrm{E}\right)^{-1}\mathrm{C}^{\mathrm{T}}\mathrm{d}\,. \tag{22}$$

The above formula allows us to evaluate K_D^* through the measurable variables collected from the time window T_{PFC}.

3.4. Implement of the Evaluation Method

According to the discussions in the above subsections, we can evaluate the FFS ability of a source via its dynamic behaviors during a frequency evaluation. The equivalent inertia constant H^* can be obtained via the data collected at T_{inertia}, and then the virtual droop constant K_D^* can be estimated following T_{PFC}. On this basis, we can obtain a complete FFS ability evaluation of the method based on the estimated H^* and K_D^*. Figure 4 illustrates the complete FFS ability evaluation process.

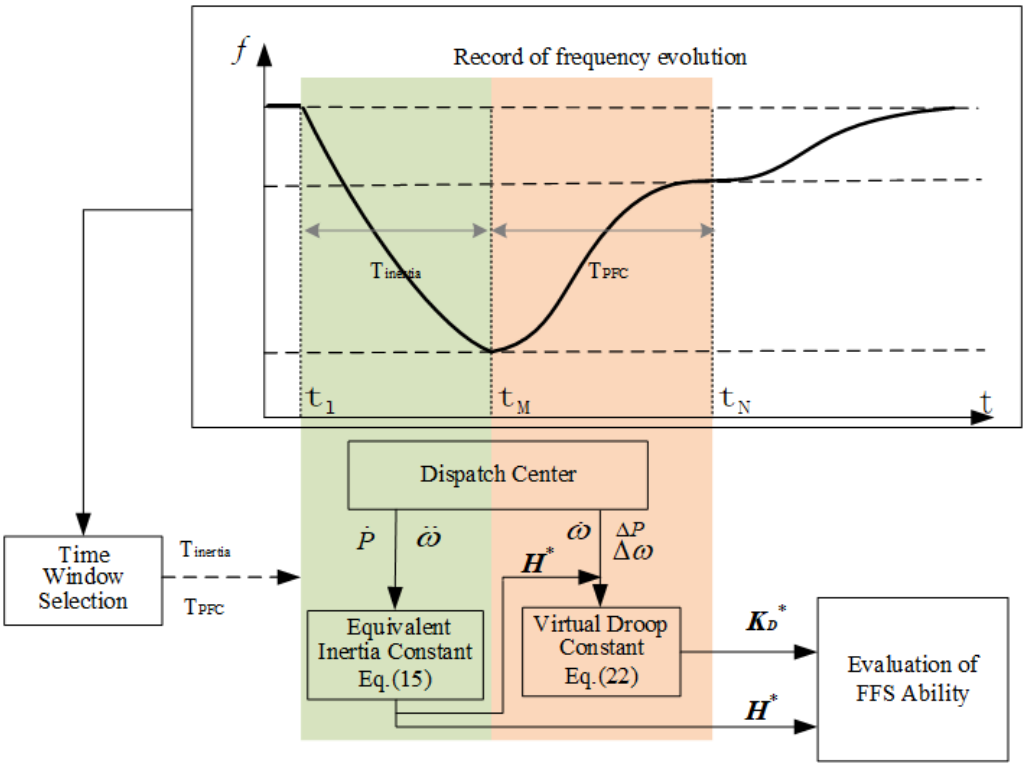

Figure 4. Evaluation flowchart.

The time window selection is based on the record of frequency evolution. However, as we can see in Figure 1, T_{inertia} and T_{PFC} are partly overlapped. In this context, the simplest method to separate the time window for evaluating H^* and K_D^* is selecting the maximal frequency deviation point during the frequency evolution as the dividing line. Therefore, the t_M and t_J above are the same time point. t_1 is the time when the frequency event occurs. The end time of the time window to evaluate K_D^*, namely, t_N, is selected as the time followed by 1 s where the frequency difference between the maximal and the minimal value at this 1 s is less than 0.01 Hz.

The datum, including the dynamic frequency and active output of the source, for the estimated equivalent inertia constant and the estimated virtual droop constant is obtained from the dispatch center within the corresponding time windows, namely, $[t_1, t_M]$ and $[t_M, t_N]$. Then, with Equations (15) and (22), we can obtain H^* and K_D^*, respectively. Then the FFS ability of the source can be reported as completed from the estimated H and K_D.

4. Case Study

This section validates the proposed FFS ability evaluation method for both the SG and IBRs, including the GFL and the GFM via the well-known 10-machine 39-bus system shown in Figure 5. The system uses PMUs with a sampling frequency of 100 Hz for data acquisition.

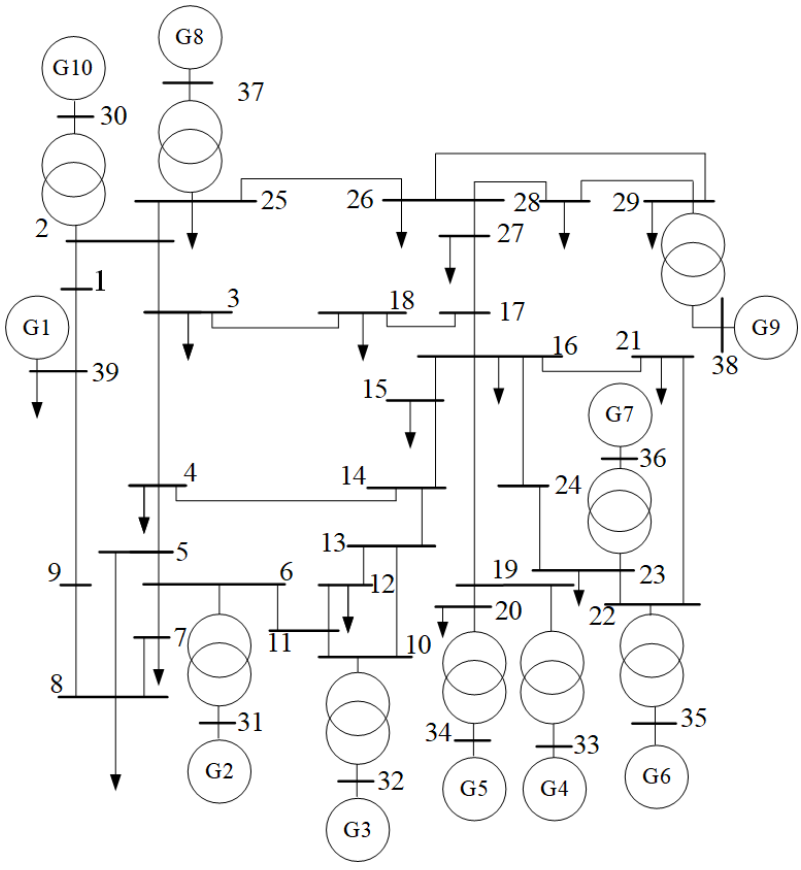

Figure 5. Ten-machine 39-bus system.

All the simulation results shown in this section are obtained by the power system analysis tool DOME [33], and the formulas for estimating the FFS indexes are solved by Lapack. Lapack is a set of functions written in Fortran for numerical computation. The relative error ξ used to represent the accuracy of the estimation shown in the remainder of the section is calculated as follows:

$$\xi = \frac{|X^* - X|}{X} \times 100\%, \tag{23}$$

where ξ is the error value, X^* is the measured value of the measured quantity, and X is the actual value of the measured quantity.

4.1. Accuracy Analysis for the Proposed Method

Considering that the inertia and droop of an SG can be accurately known and the concepts of the equivalent inertia constant and the equivalent droop constant of the IBR are deduced from the inertia and droop of the SG, this subsection validates the proposed FFS index evaluation method on estimating the inertia and the droop of the SGs in the test system.

In this subsection, we consider the following three different frequency events to show the FFS ability of the SGs:

- Scenario i: a sudden load increase;
- Scenario ii: the loss of G10;
- Scenario iii: a sudden load decrease.

The trajectories of the frequency evolution following the above events are shown in Figure 6.

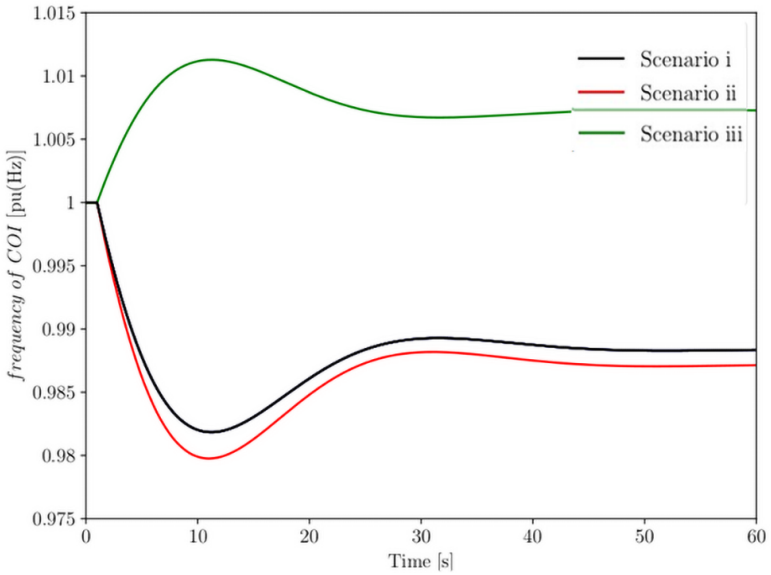

Figure 6. Evolutionary trajectories of SG frequency for three scenarios.

The time windows for the equivalent inertia constant and droop estimation for the scenarios shown in Figure 6 are the following:

- Scenario i: $t_1 = 1.00$, $t_M = 10.22$, $t_N = 48.84$;
- Scenario ii: $t_1 = 1.00$, $t_M = 9.97$, $t_N = 48.13$;
- Scenario iii: $t_1 = 1.00$, $t_M = 10.22$, $t_N = 48.43$.

The relative estimation errors of the inertia constant and droop gain of each SG are shown in Figures 7 and 8.

According to Figures 7 and 8, we can see that the relative errors of the estimation of the equivalent inertia constants are less than 0.36% for each scenario, and the relative errors of the droop estimation are less than 0.32%. The above results verify that the proposed method can accurately evaluate the equivalent inertia constant and droop of the SG. Meanwhile, the errors for the estimation results obtained from various scenarios are at a similar level, which indicates that the accuracy of the proposed evaluation method would not be affected by the type of frequency event.

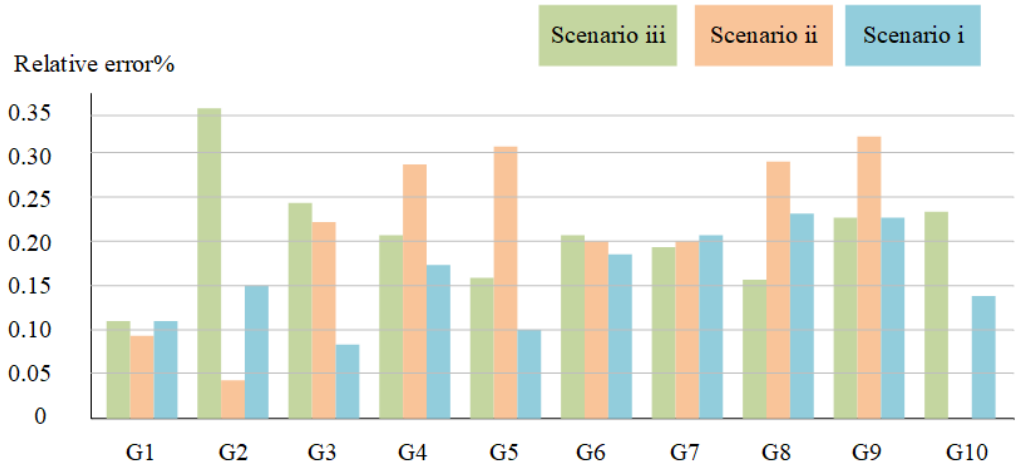

Figure 7. Evaluating the equivalent inertia constant of the SG.

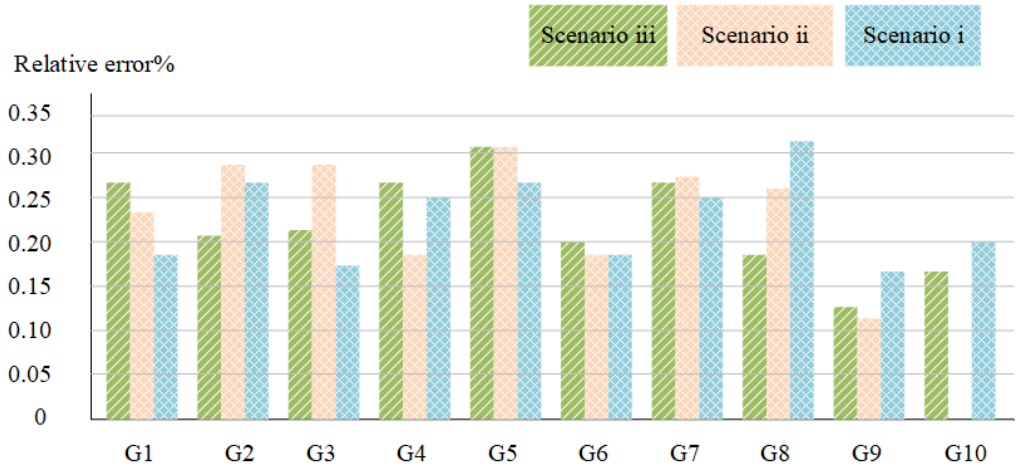

Figure 8. Evaluating the virtual droop constant of the SG.

To further validate the robustness of the proposed method against the stochastic dynamics existing in the modern power system, we consider the case that G8 and G9 are replaced by wind power plants, which leads to a 30% wind penetration of the system. The dynamic wind is modeled as a standard Weibull distribution [34]. With the stochastic behaviors of the wind, the relative errors of inertia and droop estimation at scenario i are shown in Figure 9.

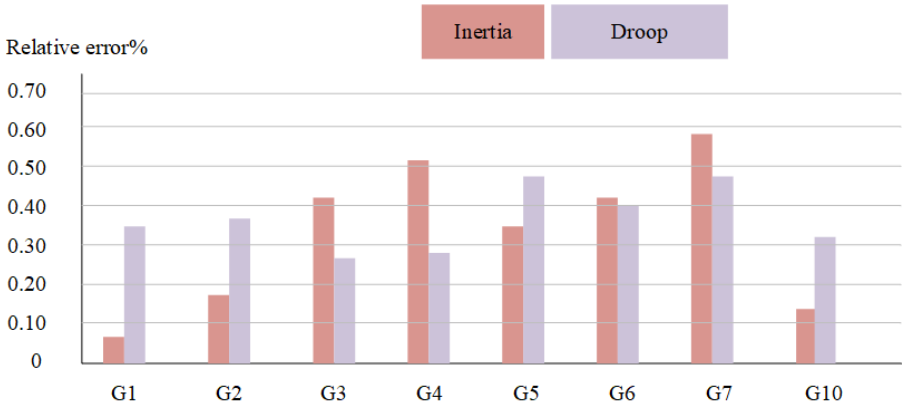

Figure 9. The results of the evaluation of the SG in a low inertia system.

Comparing Figure 9 with Figures 7 and 8, the relative error range for inertia estimation changes from [0.11–0.37] to [0.08–0.59], and the relative error range of droop estimation changes from [0.17–0.31] to [0.25–0.49]. These results indicate that the stochastic behaviors would affect the accuracy of the FFS ability estimation while still at an acceptable range.

To further understand the impact of the stochastic dynamics, Figures 10 and 11 show the inertia and droop estimation results of G7. According to these figures, the existence of wind stochastic enlarges the distribution of the data pairs used to estimate the FFS indexes but has a limited effect on the estimation result with the proposed recursive algorithm.

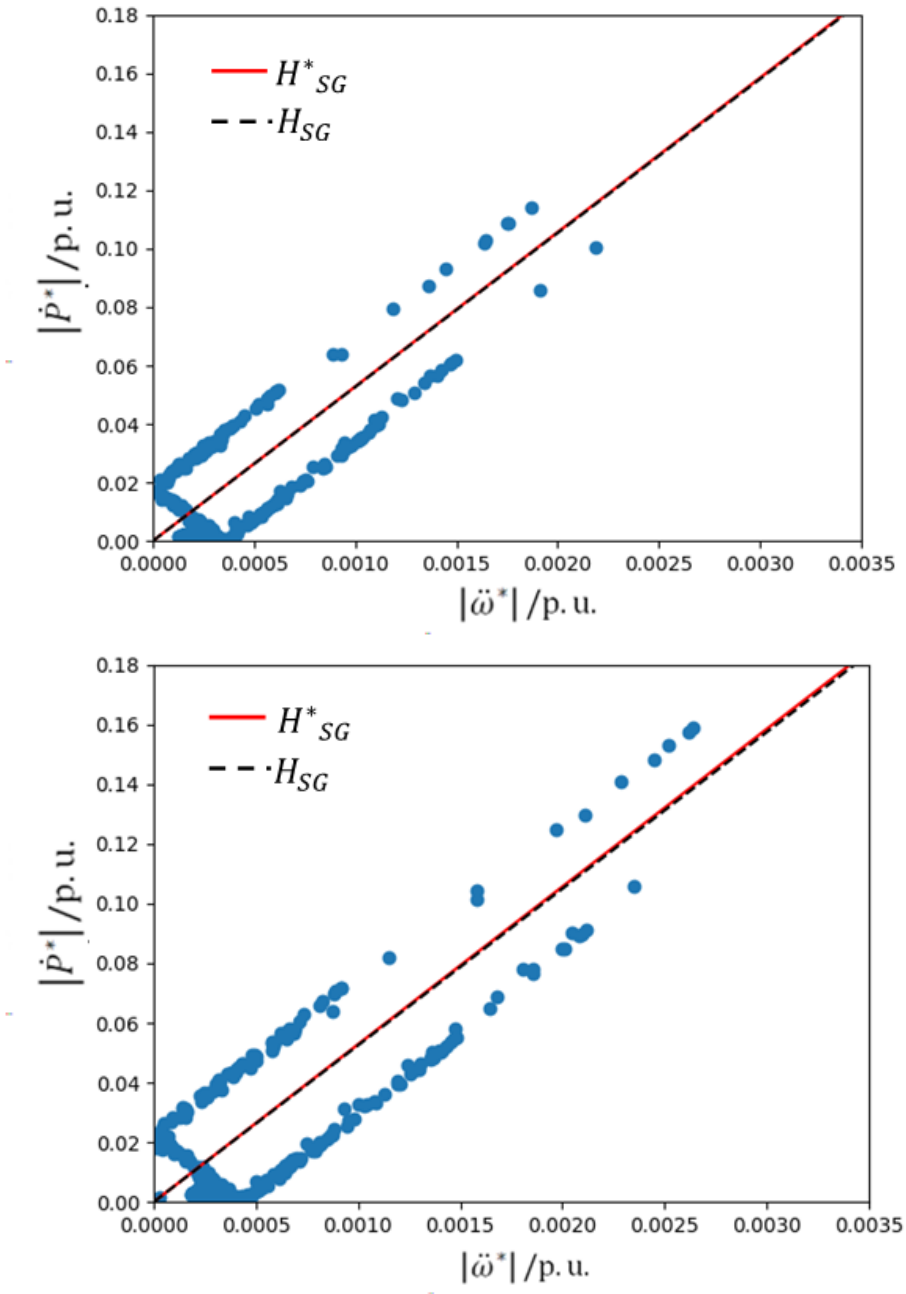

Figure 10. Equivalent inertia constant estimation of G7 under different scenarios: without wind stochastic (**upper** panel); with wind stochastic (**lower** panel).

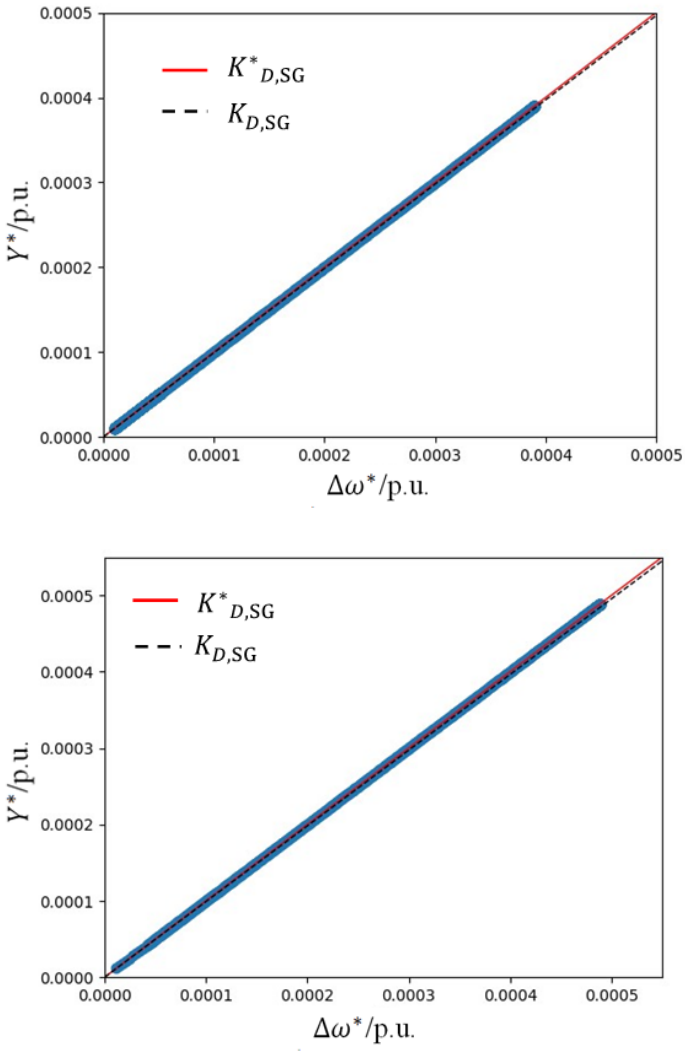

Figure 11. Equivalent droop estimation of G7 under different scenarios: without wind stochastic (**upper** panel), with wind stochastic (**lower** panel).

4.2. Analysis of the FFS Ability of the IBR

Section 4.1 validates the accuracy of the proposed FFS index evaluation method in identifying the inertia constant and droop gain of the SG. This subsection investigates the FFS ability of the GFL and GFM inverters with the proposed evaluation method.

In this subsection, we consider that G2, G3, G4, and G6 are replaced by IBRs with FFS. In scenario (a), all the IBRs are GFL. In scenario (b), all the IBRs are GFM. To compare the FFSs of the GFL and the GFM, they have identical parameters in their control loop. Table 1 lists all the parameters of the fast frequency control of the different IBRs.

Table 1. Parameters for fast frequency control of different IBRs.

Parameters	Values			
	G2	**G3**	**G4**	**G6**
K_D(GFM)/K_d(GFL)	10	15	15	10
M(GFM)/K_M(GFL)	60.6	71.6	57.2	69.6

The frequency evolution trajectories of scenarios (a) and (b) following a sudden load increase are shown in Figure 12.

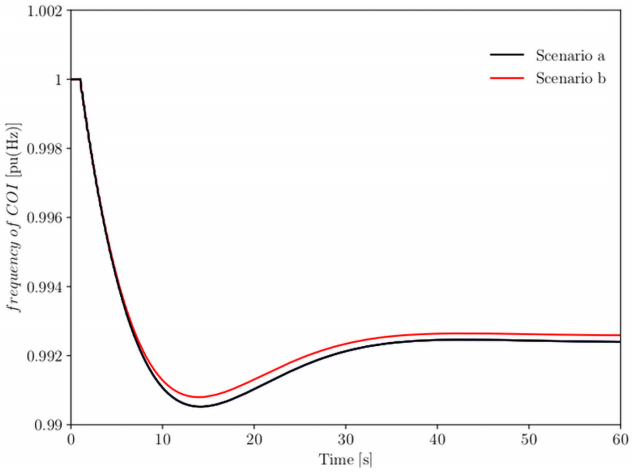

Figure 12. Frequency evolution trajectories for scenarios (a) and (b) following the loss of G10.

The maximal RoCoF scenarios (a) and (b) are 2.39 and 2.19, respectively. Additionally, the frequency nadirs of scenarios (a) and (b) are 59.41 and 59.46 Hz, respectively. The RoCoF is compared as the following formula:

$$\text{RoCoF} = 60\frac{\omega(t+\Delta t)-\omega(t)}{\Delta t}, \tag{24}$$

where ω is the angular frequency of the center of inertia (CoI) per unit, t is the simulation time, and Δt is a time step to compute the RoCoF that we select as 0.01 s. These results, as well as Figure 12, indicate that the GFM should have a stronger FFS ability compared with the GFL. Figure 13 shows the results of estimating the FFS metrics for the IBR for scenarios (a) and (b), which show the difference between the estimated FFS capacity metrics obtained by weighting the data from the two case estimation results and the control parameters listed in Table 1. The two cases are scenario (i), a sudden load increase, and scenario (ii), the loss of G10. To rule out the impact of the estimation error, we use the case with wind stochastic and we run Monte Carlo tests 500 times to obtain the mean value for the estimated equivalent inertia constant and virtual droop constant.

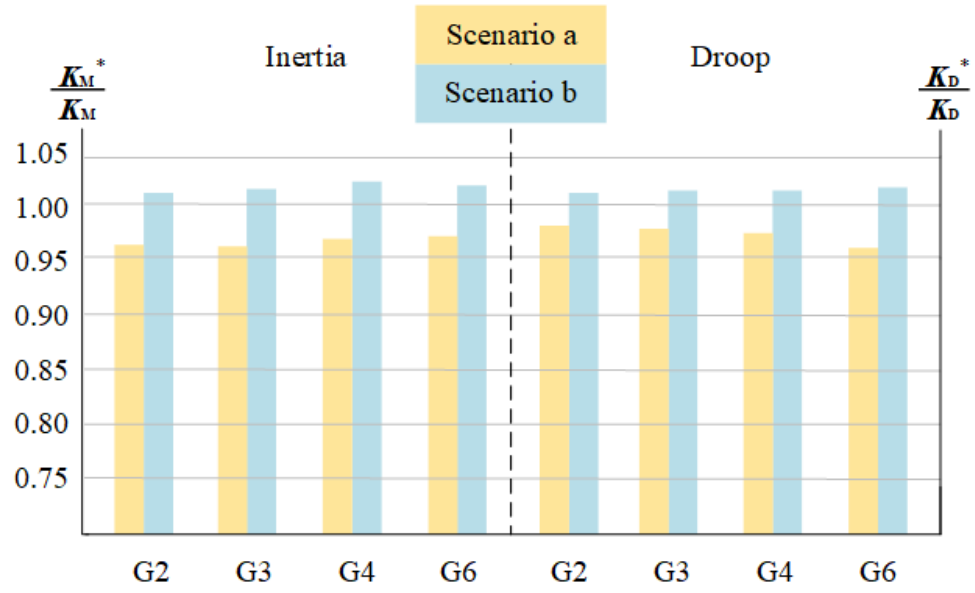

Figure 13. Results of the GFL and GFM assessment.

Figure 13 shows that all the GFMs have higher FFS ability indexes than the GFLs. This result is identical to the frequency evolution trajectories of scenarios (a) and (b). As discussed in Section 2, the reason that the GFM has a better FFS ability can be its faster frequency response due to avoiding the dynamics of the PLL.

5. Conclusions

This paper proposes an FFS ability evaluation method based on FFS ability indexes for both an SG and IBRs, including the GFL and the GFM. According to the case study, we can conclude that the accuracy of the proposed postcontingency evaluation method is robust against the type of frequency events and the type of generation units. By employing the evaluation method, the GFM performs better than the GFL with numerically identical control parameters on FFS. The future work focuses on precontingency FFS ability evaluation with the proposed indexes.

Author Contributions: Conceptualization and methodology, M.L.; validation, R.M.; formal analysis, Y.L.; resources, Z.L.; data curation, Z.Q.; writing, H.Z. All authors have read and agreed to the published version of the manuscript.

Funding: This research was funded by the State Grid Corporation of China, grant number 5100-202240026A-1-1-ZN.

Institutional Review Board Statement: Not applicable.

Informed Consent Statement: Not applicable.

Data Availability Statement: The raw data supporting the conclusions of this article will be made available by the authors on request.

Conflicts of Interest: The authors declare no conflicts of interest.

References

1. Mahmoud, K.; Astero, P.; Peltoniemi, P.; Lehtonen, M. Promising Grid-Forming VSC Control Schemes Toward Sustainable Power Systems: Comprehensive Review and Perspectives. *IEEE Access* **2022**, *10*, 130024–130039. [CrossRef]
2. Verma, P.; K, S.; Dwivedi, B. A Self-Regulating Virtual Synchronous Generator Control of Doubly Fed Induction Generator-Wind Farms. *IEEE Can. J. Electr. Comput. Eng.* **2023**, *46*, 35–43. [CrossRef]
3. Rafiee, A.; Batmani, Y.; Ahmadi, F.; Bevrani, H. Robust Load-Frequency Control in Islanded Microgrids: Virtual Synchronous Generator Concept and Quantitative Feedback Theory. *IEEE Trans. Power Syst.* **2021**, *36*, 5408–5416. [CrossRef]
4. Strunz, K.; Almunem, K.; Wulkow, C.; Kuschke, M.; Valescudero, M.; Guillaud, X. Enabling 100 Renewable Power Systems Through Power Electronic Grid-Forming Converter and Control: System Integration for Security, Stability, and Application to Europe. *Proc. IEEE* **2023**, *111*, 891–915. [CrossRef]
5. Mohammed, N.; Ravanji, M.H.; Zhou, W.; Bahrani, B. Enhanced Frequency Control for Power-Synchronized PLL-Less Grid-Following Inverters. *IEEE Open J. Ind. Electron. Soc.* **2023**, *4*, 189–204. [CrossRef]
6. Bahrani, B. Power-Synchronized Grid-Following Inverter Without a Phase-Locked Loop. *IEEE Access* **2021**, *9*, 112163–112176. [CrossRef]
7. Shen, R.; Zhong, S.; Wen, X.; An, Q.; Zheng, R.; Li, Y.; Zhao, J. Multi-agent deep reinforcement learning optimization framework for building energy system with renewable energy. *Appl. Energy* **2022**, *312*, 118724. [CrossRef]
8. Yang, L.; Chen, Y.; Qiu, Q.; Wang, J. Risk Control of Mission-Critical Systems: Abort Decision-Makings Integrating Health and Age Conditions. *IEEE Trans. Ind. Inform.* **2022**, *18*, 6887–6894. [CrossRef]
9. Cui, X.; Dong, S.; Hoke, A.; Tan, J. A Unified Metric for Fast Frequency Response in Low-Inertia Power Systems. In Proceedings of the 2023 IEEE Power & Energy Society Innovative Smart Grid Technologies Conference (ISGT), Washington, DC, USA, 16–19 January 2023; pp. 1–5. [CrossRef]
10. Binbing, W.; Abuduwayiti, X.; Yuxi, C.; Yizhi, T. RoCoF Droop Control of PMSG-Based Wind Turbines for System Inertia Response Rapidly. *IEEE Access* **2020**, *8*, 181154–181162. [CrossRef]
11. Li, H.; Qiao, Y.; Lu, Z.; Zhang, B.; Teng, F. Frequency-Constrained Stochastic Planning Towards a High Renewable Target Considering Frequency Response Support From Wind Power. *IEEE Trans. Power Syst.* **2021**, *36*, 4632–4644. [CrossRef]
12. Fang, Q.; Chen, Z.; Zou, Y.; Zhou, L.; Yin, M. Improved Stepwise Inertial Control for Wind Turbines Considering Frequency Response of Synchronous Generators. In Proceedings of the 2021 China Automation Congress (CAC), Beijing, China, 22–24 October 2021; pp. 2587–2593. [CrossRef]
13. Pulgar-Painemal, H.; Wang, Y.; Silva-Saravia, H. On Inertia Distribution, Inter-Area Oscillations and Location of Electronically-Interfaced Resources. *IEEE Trans. Power Syst.* **2018**, *33*, 995–1003. [CrossRef]

14. Liu, H.; Zhang, C.; Peng, X.; Zhang, S. Configuration of an Energy Storage System for Primary Frequency Reserve and Inertia Response of the Power Grid. *IEEE Access* **2021**, *9*, 41965–41975. [CrossRef]
15. Wang, Y.; Yokoyama, A. On-line estimation of power system inertia using short-time synchronous phasor measurements under high generator damping. In Proceedings of the 2021 International Conference on Power System Technology (POWERCON), Hainan, China, 10–11 November 22021; pp. 1919–1924. [CrossRef]
16. Guo, X.; Zhu, D.; Hu, J.; Zou, X.; Kang, Y.; Guerrero, J.M. Inertial PLL of Grid-connected Converter for Fast Frequency Support. *CSEE J. Power Energy Syst.* **2023**, *9*, 1594–1599. [CrossRef]
17. Saeedian, M.; Pournazarian, B.; Taheri, S.; Pouresmaeil, E. Provision of Synthetic Inertia Support for Converter-Dominated Weak Grids. *IEEE Syst. J.* **2022**, *16*, 2068–2077. [CrossRef]
18. Ngo, H.T.; Kamal, E.; Marinescu, B. Fast Frequency Support at a Wind Energy System Using Time-Varying Inertia and Droop Controls based on Globally Optimal H_∞ Control Design. In Proceedings of the 2021 22nd International Middle East Power Systems Conference (MEPCON), Assiut, Egypt, 14–16 December 2021; pp. 32–37. [CrossRef]
19. Ekomwenrenren, E.; Tang, Z.; Simpson-Porco, J.W.; Farantatos, E.; Patel, M.; Hooshyar, H. Hierarchical Coordinated Fast Frequency Control Using Inverter-Based Resources. *IEEE Trans. Power Syst.* **2021**, *36*, 4992–5005. [CrossRef]
20. Liu, Y.; Chen, J.; Ge, C.; Wang, K.; Chang, X.; Zhao, Q. Index System for Evaluating the Supporting Capability of the Inverter-based Resource. In Proceedings of the 2023 IEEE Power & Energy Society General Meeting (PESGM), Orlando, FL, USA, 16–20 July 2023; pp. 1–5. [CrossRef]
21. Liu, W.; Geng, G.; Jiang, Q.; Fan, H.; Yu, J. Model-Free Fast Frequency Control Support With Energy Storage System. *IEEE Trans. Power Syst.* **2020**, *35*, 3078–3086. [CrossRef]
22. Fernandez-Muñoz, D.; Guisandez, I.; Perez-Diaz, J.I.; Chazarra, M.; Femandez-Espina, A.; Burke, F. Fast Frequency Control Services in Europe. In Proceedings of the 2018 15th International Conference on the European Energy Market (EEM), Lodz, Poland, 27–29 June 2018; pp. 1–5. [CrossRef]
23. Wang, X.; Taul, M.G.; Wu, H.; Liao, Y.; Blaabjerg, F.; Harnefors, L. Grid-Synchronization Stability of Converter-Based Resources—An Overview. *IEEE Open J. Ind. Appl.* **2020**, *1*, 115–134. [CrossRef]
24. Geng, H.; He, C.; Liu, Y.; He, X.; Li, M. Overview on Transient Synchronization Stability of Renewable-rich Power Systems. *High Volt. Eng.* **2022**, *48*, 3367–3383. [CrossRef]
25. Cheema, K.M. A comprehensive review of virtual synchronous generator. *Int. J. Electr. Power Energy Syst.* **2020**, *120*, 106006. [CrossRef]
26. Kundur, P. *Power System Stability and Control*; McGraw-Hill Education: New York, NY, USA, 1994. [CrossRef]
27. Harnefors, L.; Schweizer, M.; Kukkola, J.; Routimo, M.; Hinkkanen, M.; Wang, X. Generic pll-based grid-forming control. *IEEE Trans. Power Electron.* **2022**, *37*, 1201–1204. [CrossRef]
28. Morán-Río, D.P.; Roldán-Pérez, J.; Prodanović, M.; García-Cerrada, A. Influence of the phase-locked loop on the design of microgrids formed by diesel generators and grid-forming converters. *IEEE Trans. Power Electron.* **2022**, *5*, 5122–5137. [CrossRef]
29. Milano, F.; Ortega, A.; Conejo, A.J. Model-Agnostic Linear Estimation of Generator Rotor Speeds Based on Phasor Measurement Units. *IEEE Trans. Power Syst.* **2018**, *33*, 7258–7268. https://doi.org/10.1109/TPWRS.2018.2846737.
30. Milano, F.; Ortega, A. A Method for Evaluating Frequency Regulation in an Electrical Grid—Part I: Theory. *IEEE Trans. Power Syst.* **2021**, *36*, 183–193. [CrossRef]
31. Ortega, A.; Milano, F. A Method for Evaluating Frequency Regulation in an Electrical Grid—Part II: Applications to Non-Synchronous Devices. *IEEE Trans. Power Syst.* **2021**, *36*, 194–203. [CrossRef]
32. Peng, S.; Lu, J.; Cao, J.; Peng, Q.; Yang, Z. Adaptive graph regularization method based on least square regression for clustering. *Signal Process. Image Commun.* **2023**, *114*, 116938. [CrossRef]
33. Milano, F. A python-based software tool for power system analysis. In Proceedings of the 2013 IEEE Power & Energy Society General Meeting, Vancouver, BC, Canada, 21–25 July 2013; pp. 1–5. [CrossRef]
34. Milano, F. *Power System Modelling and Scripting*; Springer: Berlin/Heidelberg, Germany, 2010. [CrossRef]